Cell adhesion and culture medium dependent changes in the high frequency mechanical vibration induced proliferation, osteogenesis, and intracellular organization of human adipose stem cells

Cell adhesion and culture medium dependent changes in the high frequency mechanical vibration induced proliferation, osteogenesis, and intracellular organization of human adipose stem cells

H.T. Halonen[a,*], T.O. Ihalainen[b], L. Hyväri[c,d], S. Miettinen[c,d], J.A.K. Hyttinen[a]

[a] *Computational Biophysics and Imaging Group, Faculty of Medicine and Health Technology, Tampere University, Arvo Ylpön katu 34, 33520, Tampere, Finland*
[b] *Cellular Biophysics Group, Faculty of Medicine and Health Technology, Tampere University, Arvo Ylpön katu 34, 33520, Tampere, Finland*
[c] *Adult Stem Cell Group, Faculty of Medicine and Health Technology, Tampere University, Arvo Ylpön katu 34, 33520, Tampere, Finland*
[d] *Research, Development and Innovation Centre, Tampere University Hospital, Biokatu 6, 33520, Tampere, Finland*

ARTICLE INFO

ABSTRACT

High frequency (HF) mechanical vibration appears beneficial for *in vitro* osteogenesis of mesenchymal stem cells (MSCs). However, the current mechanobiological understanding of the method remains insufficient. We designed high-throughput stimulators to apply horizontal or vertical high magnitude HF (HMHF; 2.5 G_{peak}, 100 Hz) vibration on human adipose stem cells (hASCs). We analyzed proliferation, alkaline phosphatase (ALP) activity, mineralization, and effects on the actin cytoskeleton and nuclei using immunocytochemical stainings. Proliferation was studied on a standard tissue culture plastic (sTCP) surface and on an adhesion supporting tissue culture plastic (asTCP) surface in basal (*BM*) and osteogenic (*OM*) culture medium conditions. We discovered that the improved cell adhesion was a prerequisite for vibration induced changes in the proliferation of hASCs. Similarly, the adhesion supporting surface enabled us to observe vibration initiated ALP activity and mineralization changes in *OM* condition. The horizontal vibration increased ALP activity, while vertical stimulation reduced ALP activity. However, mineralization was not enhanced by the HMHF vibration. We performed image-based analysis of actin and nuclei to obtain novel data of the intracellular-level responses to HF vibration in *BM* and *OM* conditions. Our quantitative results suggest that actin organizations were culture medium and stimulation direction dependent. Both stimulation directions decreased *OM* induced changes in nuclear size and elongation. Consequently, our findings of the nuclear deformations provide supportive evidence for the involvement of the nuclei in the mechanocoupling of HF vibration. Taken together, the results of this study enhanced the knowledge of the intracellular mechanisms of HF vibration induced osteogenesis of MSCs.

1. Introduction

Different types of mechanical impacts have been found to be beneficial for bone tissue *in vivo* (Verschueren et al., 2004; Nikander et al., 2009). This beneficial effect is based on mechanotransduction in which the mechanical stimuli of the environment translates into intracellular biochemical signals and changes in cell functions (Paluch et al., 2015). High frequency (*HF*, ≥ 10 Hz) mechanical vibration has been studied in directing the differentiation fate of mesenchymal stem/stromal cells (MSCs) into several different cell types (Pré et al., 2013; Bartlett et al., 2015; Kim et al., 2015; Marycz et al., 2016; Zhao et al., 2017) This method is most typically applied for the analysis of the osteogenic differentiation of MSCs (Tirkkonen et al., 2011; Kim et al., 2012; Zhang

et al., 2012; Pré et al., 2013). The majority of HF vibration studies have reported the intensified osteogenic differentiation of MSCs in osteogenic culture medium (*OM*) condition (Tirkkonen et al., 2011; Kim et al., 2012; Zhang et al., 2012; Pré et al., 2013; Uzer et al., 2013; Chen et al., 2015a; Pongkitwitoon et al., 2016; Maredziak et al., 2017; Lu et al., 2018). To date, only one study has reported unchanged alkaline phosphatase (ALP) activity (an early marker of osteogenesis) and decreased bone cell maturation (mineralization) with HF vibration (Lau et al., 2011).

A severe limitation in the existing literature is the use of highly variable stimulation parameters, a situation that calls for the optimization of the method. HF vibration has been applied at various stimulation bout durations (Sen et al., 2011; Tirkkonen et al., 2011; Kim

Abbreviations		HF	High frequency
		HMHF	High magnitude and high frequency method
ALP	Alkaline phosphatase	hBMSCs	Human bone marrow-derived mesenchymal stem cells
BM	Basal culture medium	ICC	Immunocytochemical
ECM	Extracellular matrix	LINC	Linker of Nucleoskeleton and Cytoskeleton
FAK	Focal adhesion kinase	LMHF	Low magnitude and high frequency method
FDM	Fused deposition modeling	MSCs	Mesenchymal stem/stromal cells
hASCs	human adipose stem cells	*NAR*	Nuclear aspect ratio
asTCP	Adhesion supporting tissue culture plastic	*OM*	Osteogenic culture medium
cv	Circular variance	*SD*	Standard deviation
deg$_{AVE}$	Mean orientation angle	sTCP	Standard tissue culture plastic

et al., 2012; Zhang et al., 2012; Uzer et al., 2015; Maredziak et al., 2017), over a wide frequency range (10 Hz–5 kHz), and mostly by using the low magnitude and high frequency method (LMHF, < 1 G_{peak}) (Zhang et al., 2012; Chen et al., 2015a; Pemberton et al., 2015). In a previous study by our research group, we were the first to report that the high magnitude and high frequency method (HMHF, ≥ 1 G_{peak}) was able to intensify the osteogenic differentiation of human adipose stem cells (hASCs) (Tirkkonen et al., 2011). Moreover, other studies have also confirmed our findings with MSCs (Uzer et al., 2013; Pemberton et al., 2015; Pongkitwitoon et al., 2016). In vertical HF vibration, the cell culture is moved perpendicularly to the cell adhesion. This method has dominated the field over horizontal and vertically rotating HF vibrations, where the cell cultures are moved either parallel or simultaneously perpendicularly and parallel to the cell adhesion (Reviewed in: Edwards and Reilly, 2015; McClarren and Olabisi, 2018). Interestingly, the horizontal stimulation was recently found to be more effective than vertical stimulation in directing human bone marrow-derived MSCs (hBMSCs) differentiation towards osteogenic lineage in combination with altering the actin cytoskeleton and increasing cellular stiffness (Pongkitwitoon et al., 2016).

A detailed understanding of intracellular-level responses and mechanocoupling of the HF vibration is still lacking. During HF vibration, cells experience both inertial forces and fluid shear stress in the cell culture, of which the inertial forces have been shown to be more dominant than fluid shear (Uzer et al., 2012, 2013, 2014). Previous studies have also shown that the actin cytoskeleton and cell adhesion are important regulators of MSC differentiation in static culture condition (Salasznyk et al., 2007; Kilian et al., 2010; Shih et al., 2011; Hyväri et al., 2018). Osteogenic differentiation is accompanied by the remodeling of the actin cytoskeleton (Titushkin and Cho, 2007; Yourek et al., 2007). Furthermore, HF vibration affects the actin cytoskeleton in both basal culture medium (*BM*) (Nikukar et al., 2013; Uzer et al., 2015; Zhang et al., 2015) and *OM* conditions (Demiray and Özcivici, 2015; Pongkitwitoon et al., 2016). These biochemically or mechanically induced changes in the actin result in altered mechanical properties of MSCs (Titushkin and Cho, 2007; Yourek et al., 2007; Pongkitwitoon et al., 2016). Indeed, there is some evidence that HF vibration increases the number of focal adhesions and activates focal adhesion kinase (FAK) signaling (Nikukar et al., 2013; Uzer et al., 2015). Interestingly, the HF vibration initiated proliferation of MSCs can be increased even further by supporting the cell adhesion (Uzer et al., 2013). In mechanotransduction-based HF vibration, responses are mediated into the nucleus via the interaction of the actin cytoskeleton and the nucleus through Linker of Nucleoskeleton and Cytoskeleton (LINC) complexes. HF vibration induces nuclear movement which then pulls the actin cytoskeleton and alters nucleoskeletal and actin-related gene expressions (Uzer et al., 2013, 2014, 2015; Pongkitwitoon et al., 2016). This phenomenon is also referred to as "inside-inside" signaling (Uzer et al., 2015). Here, either the disruption of the integrity of the actin cytoskeleton or the inhibiting of the coupling of the actin with nuclei through LINC complexes attenuates the vibration-induced signaling responses (Uzer et al., 2015). Although the involvement of the nucleus

in the "inside-inside" mechanocoupling of HF stimulus is known, the role of the morphological changes of the nucleus in this process is still poorly understood. To the best of our knowledge, there has only been one study that states that nuclear height increases during HF vibration (Demiray and Özcivici, 2015).

Further studies are required to elucidate the synergistic effects of mechanical stimulation and biochemical culture conditions in order to gain a better understanding of the mechanocoupling of HF vibration. In this study, our aim was to investigate the effects of horizontal and vertical HMHF vibration on hASC proliferation, osteogenic differentiation, the remodeling of the actin cytoskeleton, and nuclear deformations. To reach our aim, we developed high-throughput cell stimulators consisting of custom-made three-dimensional (3D) printed sample vehicles compatible with commercial culture plates for long-term use in incubator conditions. 3D printing increases the flexibility to design and manufacture desirable and tailored products for medicine, such as prostheses, implants, and 3D bioprinted scaffolds (Dodziuk, 2016; Cui et al., 2017), and the design of low-cost cell culture platforms to provide samples with dynamic tension (Raveling et al., 2018) and HF vibration (Halonen et al., 2020). We cultured hASCs on two different surfaces (standard and adhesion supporting) to enhance our knowledge of the significance of cell adhesion in HF vibration. Further, we analyzed cell proliferation in *BM* and *OM* conditions, and osteogenic differentiation in *OM* condition by analyzing ALP activity and mineralization. We also used immunocytochemistry to study the intracellular structures of the confluent hASCs on the adhesion supporting surface. This is the first study to compare how the HF vibration direction effecs the actin cytoskeleton and the nuclei of hASCs that have been cultured in osteogenically induced or control culture conditions. Our findings provide tools that can be used for the optimization of HF vibration, resulting in the significantly improved *in vitro* osteogenesis of MSCs.

2. Materials and methods

2.1. Adipose stem cell characterization and preculture

In the experiments, hASCs (passage 3–6) from four donors were used. The study was conducted in accordance with the Ethics Committee of the Pirkanmaa Hospital District, Finland (R03058). The hASCs used in this study were characterized as MSCs by flow cytometry (FACSAria; BD Biosciences, Erembodegem, Belgium). The cells were single stained at passage 1 (10 000 cells per sample) using monoclonal antibodies against CD14-PE-Cy7, CD19-PE-Cy7, CD45R0-APC, CD73-PE, CD90-APC (BD Biosciences Franklin Lakes, NJ, USA), CD105-PE (R &D Systems, Minneapolis, MN, USA), CD34-APC, and HLA-DR-PE (ImmunoTools, Friesoythe, Germany). Unstained samples were used to compensate for the background autofluorescence.

Cells were expanded in *BM* condition, consisting of DMEM/F-12 (1:1) (1x) (Invitrogen, Thermo Fisher Scientific, MA, USA), 5% human serum (PAA Laboratories Gmbh, Austria; or Biowest, France), 1% L-glutamine (GlutaMAX™, Invitrogen), and 1% PEN-STREP antibiotics (BioWhittaker™, Lonza, Switzerland), as described in our previous

study (Tirkkonen et al., 2011). The hASCs were plated in *BM* (1 ml) on a standard tissue culture plastic (sTCP) surface (Thermo Scientific™ Nunc™ Cell-Culture Treated Multidish, Thermo Scientific™; donors 1, 2; 300 cells/1.8 cm²) or on an adhesion supporting tissue culture plastic (asTCP) surface (Corning® CellBIND® Cell Culture Multiwell Plate, Sigma-Aldrich, MO, USA; donors 3, 4; 300 cells/1.9 cm²), which, according to the manufacturer, improves cell adhesion and cell proliferation when compared with the sTCP surface (Pardo et al., 2005).

2.2. HMHF vibration experiments

We manufactured light-weight sample vehicles of polylactic acid with 3D printing (Ultimaker Original, Ultimaker B.V., Netherlands), using fused deposition modeling (FDM). The sample vehicles (coated with epoxy) were designed to accept five commercial cell culture plates each, allowing for the HF vibration of large sample sizes inside the cell culture incubator. Two days after the preculture in the cell culture plates, the culture medium was replaced with fresh *BM* or *OM* consisting of *BM* supplemented with 10 mM β-glycerophosphate (Sigma-Aldrich), 0.2 mM L-ascorbic acid (Sigma-Aldrich), and 5 nM dexamethasone (Sigma-Aldrich). Thereafter, the cell culture plates were placed into the sample vehicles, which were then assembled to the specially designed supportive structures and commercial subwoofers, as shown in Fig. 1A. The daily stimulation was produced inside the cell incubators (Fig. 1B). To ensure adequate HMHF vibration, at least two measurements were taken during the stimulation start-up after culture medium change. In addition, occasional measurements were taken between the medium change intervals. To evaluate the accuracy of the mechanical vibration, we first averaged the measurement data from the individual stimulation days. Then, we averaged the daily values to
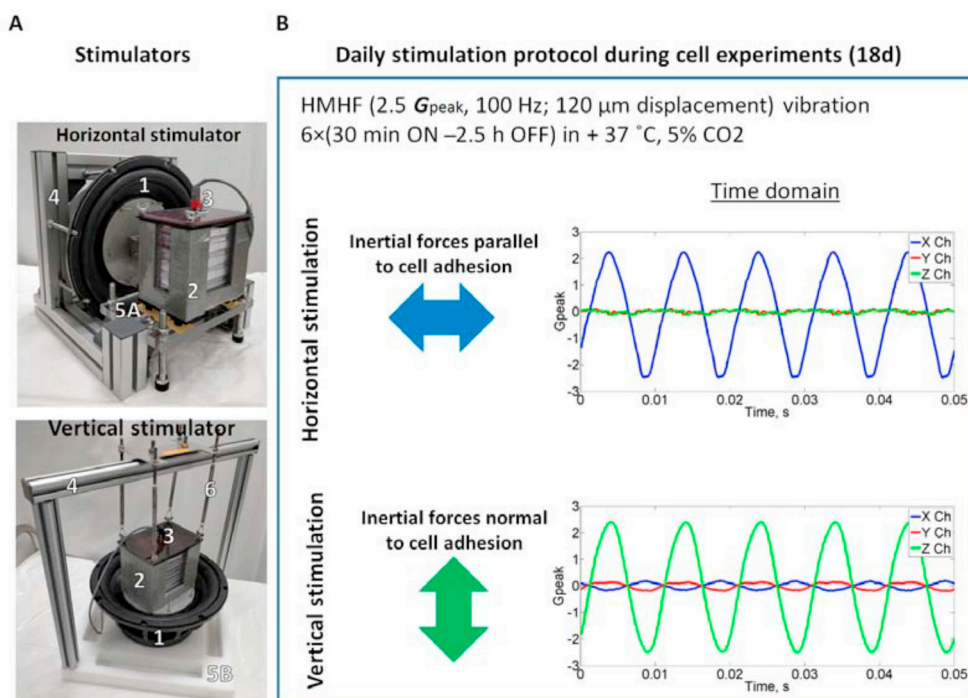

Fig. 1. The hASCs experienced different long-term mechanical stimuli in the controlled cell culture environment. (A): Commercial subwoofers (1) produced linearly accelerating movement of the 3D printed sample vehicles (2), which was measured with an accelerometer (3). Aluminum profiles (4) were used to build supportive structures for the stimulator systems. A thick plastic plate was added to the horizontal system (5A) to enable the sample vehicle to slide on wheels and to the vertical system (5B) to avoid mechanical resonances on the incubator shelf. Springs (6) supported the sample vehicle movement of the vertical system. (B): The hASC monolayers were stimulated with sinusoidal HMHF vibration in opposite directions with respect to cell adhesion. (C): The stimulators performed precisely and accurately during the long-term experiments. (D): Time line presenting the experiments and analysis time points of the study.
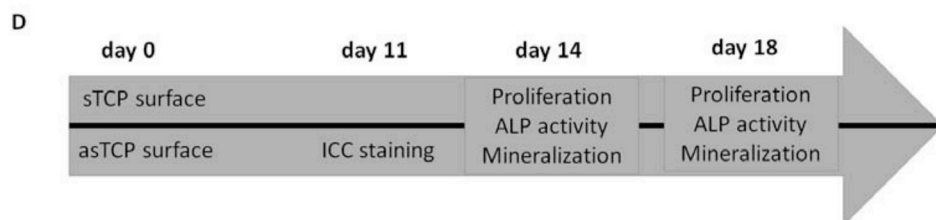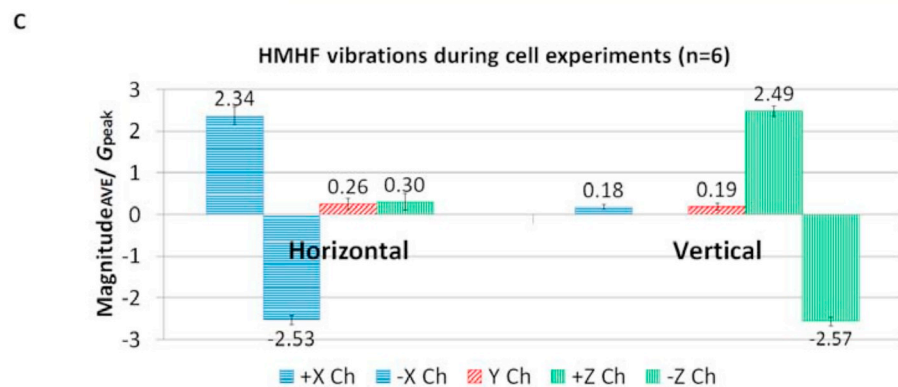
represent the data of the long-term stimulation experiment. Finally, we averaged the data of the separate stimulation experiments to better evaluate the precision of the HMHF vibration between the stimulation experiments (Fig. 1C). The culture medium was changed after 3–4 days, and the cellular responses were studied at different analysis time points (Fig. 1 D).

2.3. Proliferation and ALP activity

The hASCs were cultured on sTCP (donors 1, 2) and asTCP (donors 3, 4) surfaces for 14 days and 18 days in *BM* and *OM* conditions. Proliferation and ALP activity were studied as previously described (Tirkkonen et al., 2013). Briefly, the samples were lysed in 0.1% triton-x-100 (Sigma-Aldrich), followed by freezing of the samples ($-80\,°C$). To study proliferation, the samples were mixed with GR dye and lysis buffer of the CyQUANT® Cell Proliferation Assay Kit (Invitrogen Molecular Probes™). Fluorescences were measured with a multiplate reader (Victor 1420 Multilabel Counter, Wallac, Finland) at 480/520 nm. The same samples were used for the analysis of ALP activity, but only those samples cultured in *OM* condition were analyzed. To study ALP activity, the samples were mixed with a 1:1 working solution of 10.8 mM Sigma 104® phosphatase substrate in H_2O (Sigma-Aldrich) and 1.5 M Alkaline Buffer solution (Sigma-Aldrich). After incubation (15 min, 37 °C), the reaction was stopped using 1.0 M NaOH (Sigma-Aldrich). Absorbances were measured with a multiplate reader (Victor 1420 Multilabel Counter) at 405 nm. ALP activity was normalized with cell number.

2.4. Mineralization

The mineralization of hASCs, cultured for 14 days or 18 days on sTCP (donors 1, 2) and asTCP (donors 3, 4) surfaces in *OM* condition, was studied using Alizarin Red (AR) S staining as previously described (Hyväri et al., 2018). After a single 1 × PBS rinse, the hASCs were fixed with ice-cold 70% EtOH (60 min, $-20\,°C$) followed by staining with 2% Alizarin Red S solution (pH 4.1 to 4.3, Sigma-Aldrich) (10 min, RT). The wells were then rinsed several times and photographed (CANON, Digital ixus 100 IS 12.1Mpix, Japan) after drying. The dye was extracted with 100 mM cetylpyridinium chloride (Sigma-Aldrich) (3 h, RT), and the absorbances were measured with a multiplate reader (Victor 1420 Multilabel Counter) at 544 nm.

2.5. Immunocytochemical staining

The hASCs cultured on an asTCP surface (donors 3, 4) in *BM* and *OM* conditions were studied with immunocytochemical (ICC) staining at the day 11 time point. First, the culture medium was removed. Then, the samples were rinsed twice with 1 × PBS, fixed (4% PFA; 15–30 min, RT, dark), and rinsed three times with 1 × PBS. The ICC stain protocol comprised permeabilization (0.1% triton-x-100, Sigma-Aldrich; 15 min, RT) followed by a single 1 × PBS rinse. The samples were then blocked (1% BSA, Sigma-Aldrich; 1 h, + 4 °C) and rinsed four times with 1 × PBS. For the staining of the actin cytoskeleton, the samples were stained with phalloidin (1/100 Phalloidin-Tetramethylrhodamine B isothiocyanate (Phalloidin-TRITC, Sigma-Aldrich) in 1% BSA). The samples were then rinsed either three times with 1 × PBS and once with H_2O before embedding (VECTASHIELD Antifade Medium with DAPI, Vector Laboratories, CA, USA), or they were rinsed twice with 1 × PBS and once with DAPI (1/2000 4',6-diamidino-2-phenylindole dihydrochloride (Sigma-Aldrich) in H_2O; 5 min, RT, dark) followed by a single 1 × PBS rinse and three rinses with H_2O.

2.6. Imaging

The ICC stained samples were imaged with an inverted microscope (20 × , Olympus 1X51, Olympus Corporation of the Americas, PA, USA). Five parallel images of the sample were imaged with manually adjusted light exposure times for phalloidin-TRITC (510–550 nm) and DAPI (420 nm).

2.7. Image processing and analysis

Before analysis, the phalloidin-TRITC and DAPI images were pre-processed with the image processing package Fiji to remove background and to adjust the brightness and contrast automatically. The phalloidin-TRITC-stained images were then analyzed with an automated software tool (CytoSpectre 1.0, Kartasalo et al., 2015) to evaluate the stimulation effects on the actin cytoskeleton. After visual evaluation of the images and the analysis results (circular variance, kurtosis, and skewness), we set boundary values to classify the actin cytoskeleton into aligned, criss-crossed, or randomly organized structures (Supplementary Table 1 and Fig. 1). To present differences in the actin cytoskeleton, the data were normalized with a combined image number of the culture condition of the three experiments. Applying the methods of Berens, 2009, we wrote a matlab-script (MATLAB R2014a, MathWorks, MA, USA) to study whether the parallel-aligned actin structures changed their orientations (mean orientation angle (deg_{AVE}), circular variance (cv), and kurtosis) in any of the culture conditions. Additionally, the coherency of the parallel-aligned actin filaments were studied using the kurtosis values alone by calculating the mean kurtosis and standard deviation (*SD*) from the parallel images of the culture condition.

We analyzed the culture condition effects on cross-sectional nuclear area and nuclear aspect ratio (*NAR*). The DAPI-stained images were preprocessed and segmented with Fiji. Based on the visual observation of the segmented images, we set boundary values (80–1130 μm^2) for the nuclei, when analyzing the nuclear morphology (Supplementary Fig. 2). Distributions of the nuclear area and *NAR* in each culture condition were presented as histograms in which we chose binning widths of 30 μm for the cross-sectional nuclear area and 0.25 for *NAR*, similarly to Heo et al. (2016). The data of the histograms were normalized with total nuclei counts in the culture condition. For the statistical analysis of the culture effects on the nuclear area and *NAR*, the nuclei with an area exceeding boundary value (mean + 2 *SD*) were excluded because they were considered outliers similarly to Lavrov and Smirnikhina (2010). These boundaries were determined separately in *BM* (445 μm^2) and *OM* (382 μm^2) conditions, according to the maximum values among the mechanical conditions (Supplementary Table 2).

2.8. Statistical analysis

Statistical significances were analyzed in the samples cultured in static, horizontal stimulation, and vertical stimulation culture conditions separately within each media (*BM* or *OM*) and surface (sTCP or asTCP). N values of data represent the number of parallel samples/images. Quantitative results of proliferation, ALP activity, and mineralization are presented as scatter plots combined with medians given for each donor. Actin organizations (parallel-aligned, criss-crossed, random) are presented as stacked column describing mean and *SD* of the experiments. Orientations of the parallel actin are presented as rose plots, while the coherency of the parallel-aligned actin filaments is presented as mean and *SD*. The nuclear morphology (cross-sectional area, *NAR*) distributions of the culture conditions are presented as histograms of the parallel images, and data lacking + 2 *SD* outliers are presented as box plots. The statistical analyses for proliferation, ALP,

mineralization, *NAR*, cross-sectional nuclear area, and kurtosis of the parallel-aligned actin filaments were performed with SPSS Statistics (v 23, IBM, NY, USA) using Kruskall-Wallis test (One-way ANOVA on ranks) followed by Mann-Whitney U test with Bonferroni adjustment (n = 3) to make a pairwise comparison between the mechanical conditions in each adhesion surface. Orientations of the parallel-aligned actin structures were tested with MATLAB R2014a (MathWorks) using omnibus test similarly to Berens, 2009. Statistically significant p-values were illustrated as < 0.05, < 0.01, and < 0.001.

3. Results

3.1. Adipose stem cell characterization

The mesenchymal origin of the hASCs was confirmed by analyzing their immunophenotype according to the criteria defined by the International Society for Cellular Therapy (Dominici et al., 2006). The hASCs were characterized as MSCs due to positive expressions of CD73, CD90, and CD105, and the lack of CD14, CD19, CD45, and HLA-DR
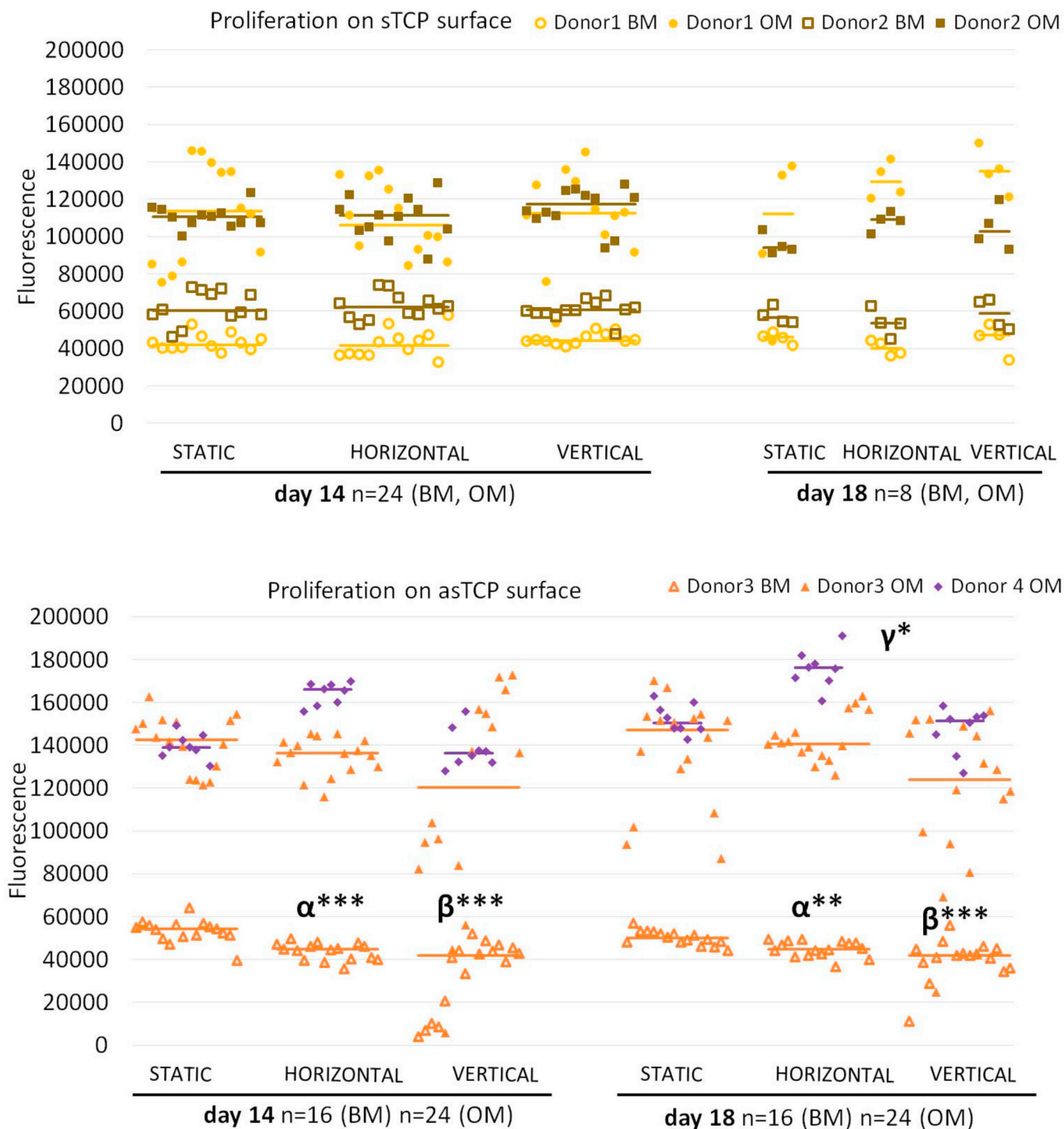
Fig. 2. Proliferation of the hASCs cultured on the sTCP and asTCP surfaces were studied in *BM* and *OM* conditions using the CyQUANT method at 14 days and 18 days. Data are presented as scatter plots and median of donors. Comparisons are made between the static culture and HMHF vibrated conditions (α, horizontal; β vertical) and between the horizontal and vertical stimulation conditions (γ). *, p < 0.05, **, p < 0.01, ***, p < 0.001.
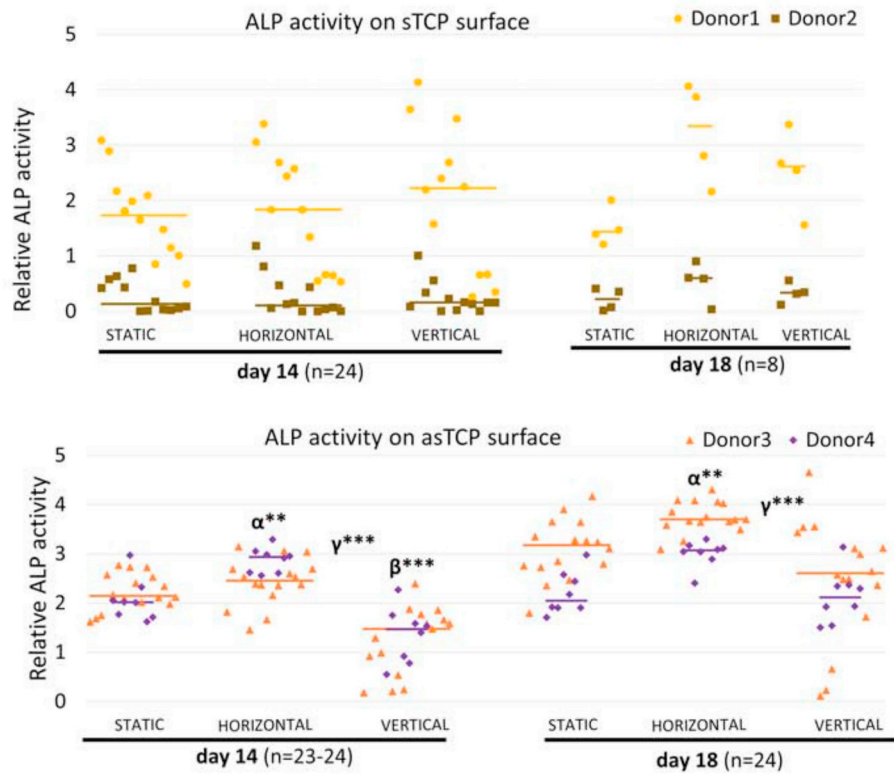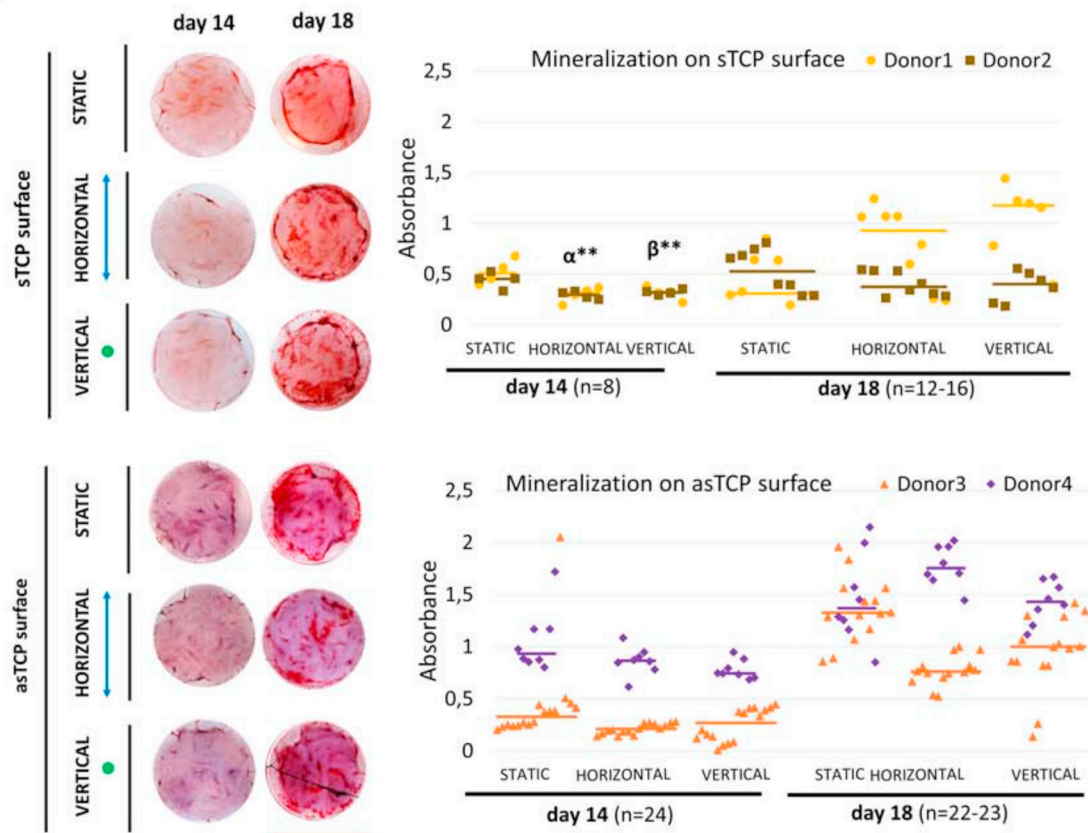
(caption on next page)

Fig. 3. Osteogenic differentiation of the hASCs in static culture, horizontal stimulation, and vertical stimulation conditions in *OM* on the sTCP and asTCP surfaces at 14 days and 18 days. (A): Cell number-normalized ALP activity results presented relative to mean of 14 days static culture condition on the sTCP surface (donors 1, 2). Data are presented as scatter plots and median of donors. (B): Representative images of AR stained samples (red dye represents Ca^{2+} salt accumulation), and quantitative mineralization results (donor 1 on sTCP surface, donor 3 on asTCP surface). Stimulation directions with respect to the wells are illustrated with a blue arrow (horizontal) and a green dot (vertical). Scale bar = 15.6 mm (red line). Data are presented similarly to ALP activity. Comparisons are made between the static culture and HMHF vibrated conditions (α, horizontal; β vertical) and between the horizontal and vertical stimulation conditions (γ). **, p < 0.01, ***, p < 0.001. (For interpretation of the references to colour in this figure legend, the reader is referred to the Web version of this article.)

expressions (Supplementary Table 3). The expression of CD34 was moderate, which has previously been associated with the early passage of the hASCs (Varma et al., 2007).

3.2. Cell proliferation

On the sTCP surface, HMHF vibration had no effect on hASC proliferation (donors 1, 2; p > 0.05) (Fig. 2). The asTCP surface supported proliferation of the hASCs in *OM* static culture condition, and the cell number at 14 days was approximately 126% higher (mean of donor medians) on the asTCP surface compared with the sTCP surface. On the asTCP surface, the HMHF vibration inhibited proliferation in *BM* condition (donor 3) both at 14 days ($p = 1 \times 10^{-5}$ for horizontal, $p = 6 \times 10^{-5}$ for vertical) and at 18 days ($p = 0.001$ for horizontal, $p = 7 \times 10^{-6}$ for vertical), especially when applied vertically. In *OM* condition, the vertical stimulation decreased proliferation significantly at 18 days when compared with the horizontal stimulation (donors 3, 4; $p = 0.01$).

3.3. Osteogenic differentiation

The ALP activity was studied after 14 days and 18 days of cell culture because of the low initial plating density of the hASCs. At 14 days, the ALP activity of the hASCs cultured in static culture condition was 151% higher on the asTCP surface than on the sTCP surface. By 18 days, the ALP activity of the hASCs cultured in static culture condition on the asTCP surface increased to 125% (mean of donor medians) of the ALP activity at 14 days, whereas the value on the sTCP surface was only 89% of the ALP activity at 14 days (Fig. 3A). The culture surface also had an effect on how the ALP activity of the hASCs responded to the HMHF vibration. Despite the modest increases especially by the horizontal stimulation when compared with the static culture condition, ALP activity remained on the sTCP surface unaffected by HMHF vibration (donors 1, 2; p > 0.05) at 18 days. Opposing effects with the stimulation directions of the HMHF vibration were revealed on the asTCP surface (donors 3, 4). The horizontal stimulation led to a statistically significant increase in ALP activity when compared with the static culture condition at 14 days ($p = 0.006$) and 18 days ($p = 0.001$). However, the vertical stimulation had a significantly decreasing effect at 14 days ($p = 9 \times 10^{-6}$), and additionally the ALP activity was decreased when compared with the horizontal stimulation at both time points (p < 0.001). At 14 days, the horizontal and vertical stimulation decreased the matrix mineralization, especially on the sTCP surface (donors 1, 2; $p = 0.002$), while on the asTCP surface this effect was only modest (donors 3, 4; $p = 0.08$) (Fig. 3B). However, at 18 days the effects of HMHF vibration on mineralization varied.

3.4. Organization of actin cytoskeleton

We performed phalloidin-TRITC staining at 11 days to observe the actin cytoskeleton after we observed that HMHF vibration had an effect on proliferation (Fig. 2) and the ALP activity (Fig. 3A) of the hASCs on the asTCP surface. Actin (donors 3, 4) were categorized into three subgroups (parallel-aligned, criss-crossed, random) (Fig. 4A). The actin cytoskeleton remained mostly parallel-aligned in all culture conditions, but in *OM* condition the actin became more criss-crossed with the resultant cost of random organization in all other mechanical conditions

except in the vertically stimulated conditions (Fig. 4B). Next, we concentrated on the effects on the parallel-aligned actin filaments. The hASCs did not orientate to any orientation angle in any of the culture conditions ($\deg_{AVE}$: p > 0.05) (Fig. 4C). However, the hASCs became more perpendicularly oriented in *BM* condition (20° to 35°, 145° to 160°) with the horizontal stimulation (90°), whereas their alignment became more parallel in *OM* condition (45° to 150°). Based on kurtosis values, the parallel-aligned actin filaments of the vertically stimulated hASCs became less coherently aligned when compared with static culture ($p = 0.005$ for *BM*, $p = 2 \times 10^{-5}$ for *OM*) and horizontal stimulation ($p = 0.03$ for *BM*, $p = 0.03$ for *OM*) conditions (Fig. 4D).
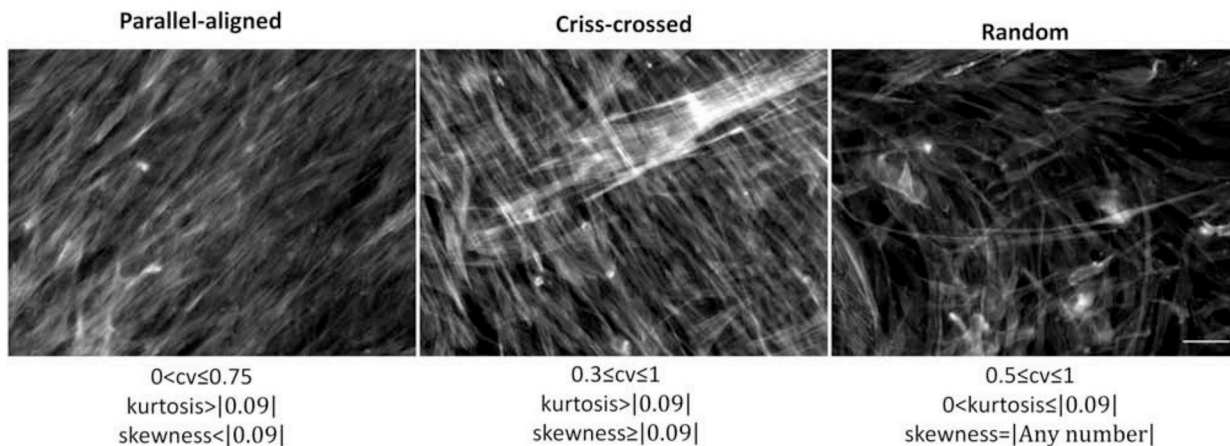
3.5. Nuclear morphology

We studied the HMHF vibration effects on the DAPI-stained nuclei of the hASCs when cultured on the asTCP surface (representative images in Supplementary Fig. 3). The cross-sectional nuclear areas were more evenly distributed in the *BM* condition histogram, indicating a larger deviation of the nuclear size in this condition (Fig. 5A). The histogram of the nuclear area was more peaked in *OM* condition than in *BM* condition. In *OM* condition, the static condition contained more similar sized nuclei, while in the mechanically treated conditions the dominant nuclei sizes had larger distributions. The histograms demonstrated skewness of the nuclear area towards the upper outliers. Nuclear aspect ratio (*NAR*), indicating the elongation of the nuclei, distributed similarly in both *BM* and *OM* conditions. In general, the nuclei were smaller and more elongated in the static culture condition of *OM* condition (150 μm², 2.00) than in *BM* condition (180 μm², 1.75). To analyze the statistical differences in nuclear size and elongation, we excluded the upper outliers (> + 2 *SD* mean cross-sectional nuclear area) (Fig. 5B). The culture medium affected the nuclear area and *NAR* both in the static culture condition and in the HMHF vibrated culture conditions. In the static culture, the nuclei were smaller (-16%) and more elongated ($+7\%$) in *OM* condition than in *BM* condition. In *BM* condition, the horizontal stimulation modestly increased both the nuclear area ($+3\%$, $p = 0.0002$) and elongation ($+4\%$, $p = 3 \times 10^{-6}$) when compared with static culture condition. In *OM* condition, both stimulation directions slightly increased the nuclear area ($+4\%$, $p = 4 \times 10^{-10}$ for horizontal, $p = 2 \times 10^{-9}$ for vertical) and decreased the nuclear elongation (-6%, $p = 6 \times 10^{-27}$ for horizontal, $p = 1 \times 10^{-20}$ for vertical) when compared with the static culture condition.

4. Discussion

Mechanical HF vibration has previously been studied in the context of osteogenic differentiation of MSCs (Tirkkonen et al., 2011; Kim et al., 2012; Zhang et al., 2012; Pré et al., 2013), and the horizontal stimulation was recently reported superior compared with the vertical vibration in influencing the proliferation, osteogenic differentiation, and mechanical properties of hBMSCs (Pongkitwitoon et al., 2016). Currently, studies on the mechanocoupling of HF vibration and its effects on the intracellular structures have mostly concentrated on the imminent stimulation effects (Uzer et al., 2015; Zhang et al., 2015; Pongkitwitoon et al., 2016). Thus, there is a lack of information on the ongoing differentiation process. Another shortcoming of prior research is that the experiments have mostly been conducted in *BM* condition
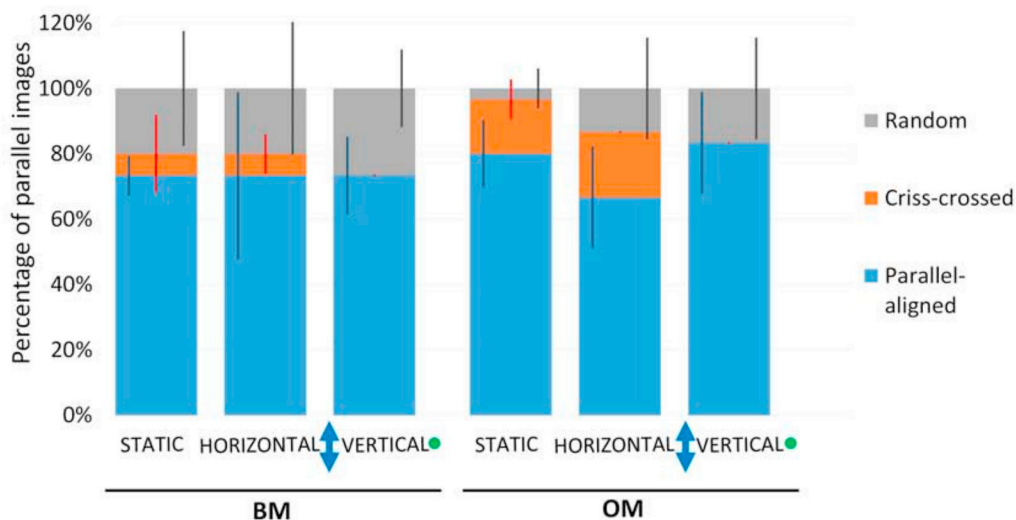
A Actin organizations

Parallel-aligned | Criss-crossed | Random

0<cv≤0.75
kurtosis>|0.09|
skewness<|0.09|

0.3≤cv≤1
kurtosis>|0.09|
skewness≥|0.09|

0.5≤cv≤1
0<kurtosis≤|0.09|
skewness=|Any number|

B Effects of culture conditions on actin organizations

C Orientations of the parallel-aligned actin structures

MECHANICAL CONDITION EFFECTS

STATIC | HORIZONTAL | VERTICAL

BM
deg_AVE=58° (n=18)
cv=0.98 (p=0.97)

deg_AVE=26° (n=17)
cv=0.82 (p=0.66)

deg_AVE=95° (n=18)
cv=0.85 (p=0.85)

OM
deg_AVE=36° (n=20)
cv=0.76 (p=0.11)

deg_AVE=88° (n=16)
cv=0.68 (p=0.44)

deg_AVE=74° (n=20)
cv=0.78 (p=0.59)
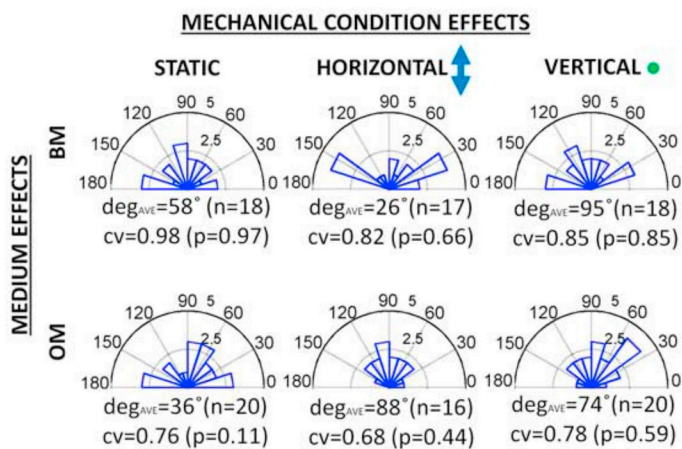
D Coherency in the actin filament alignment
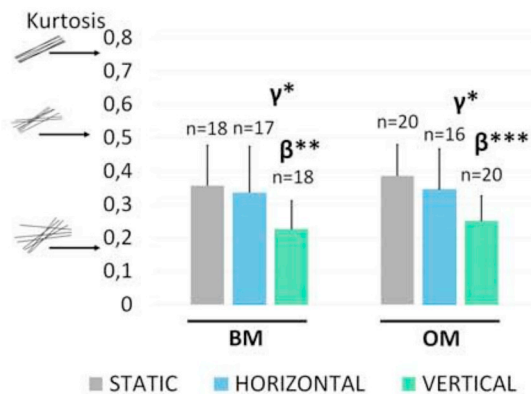
(caption on next page)

Fig. 4. Organization of the actin cytoskeleton of the hASCs in static culture, horizontal stimulation, and vertical stimulation conditions in *BM* and *OM* on asTCP surface at day 11. (A): Representative images of the parallel-aligned, criss-crossed, or random actin structures, classified based on the circular variance (cv), kurtosis, and skewness values of the phalloidin-TRITC stained images presented in static *OM* condition. Scale bar 50 µm. (B): The relative numbers of the above-mentioned actin structures, normalized with total image count of the parallel images (donor 3: n = 15, donor 4: n = 10). Data in the culture conditions are presented as a stacked column of mean and *SD* of the actin structures in three experiments. (C): Rose plots presenting the parallel-aligned actin orientation angles. Data are presented as the average orientation angle (deg$_{AVE}$) of the parallel-aligned actin structure images, number of the images (n), and circular variance (cv) and p-value of the orientations. Stimulation directions are visualized with a blue arrow (horizontal) and a green dot (vertical). (D): Kurtosis-determined differences in the actin filament alignment coherencies, independent of the orientation angles. Data are presented as mean and *SD* of kurtosis, combined with the number of the parallel images (n). Comparisons are made between the static culture and HMHF vibrated conditions (α, horizontal; β vertical) and between the horizontal and vertical stimulation conditions (γ). *, p < 0.05, **, p < 0.01, ***, p < 0.001. (For interpretation of the references to colour in this figure legend, the reader is referred to the Web version of this article.)
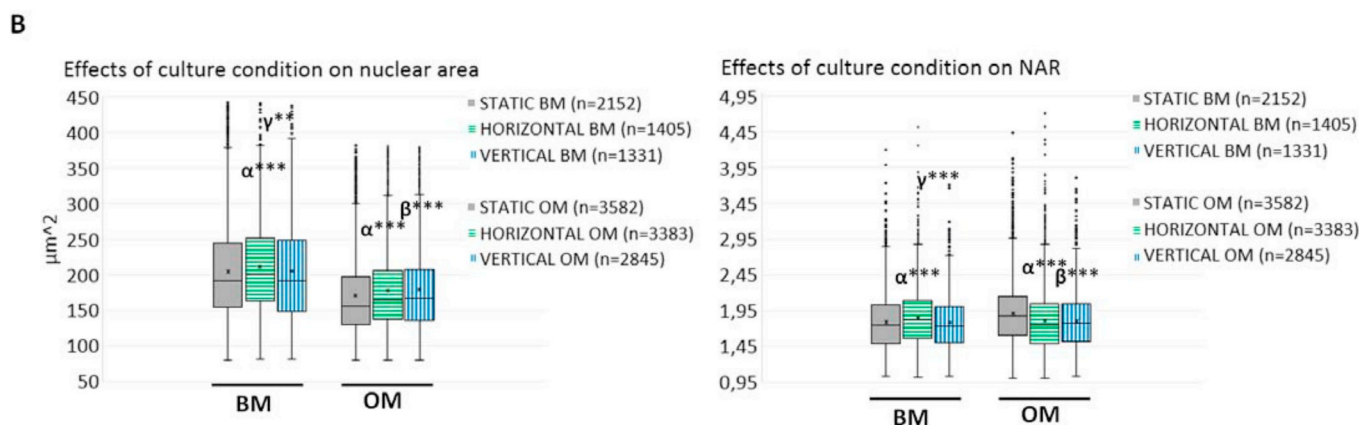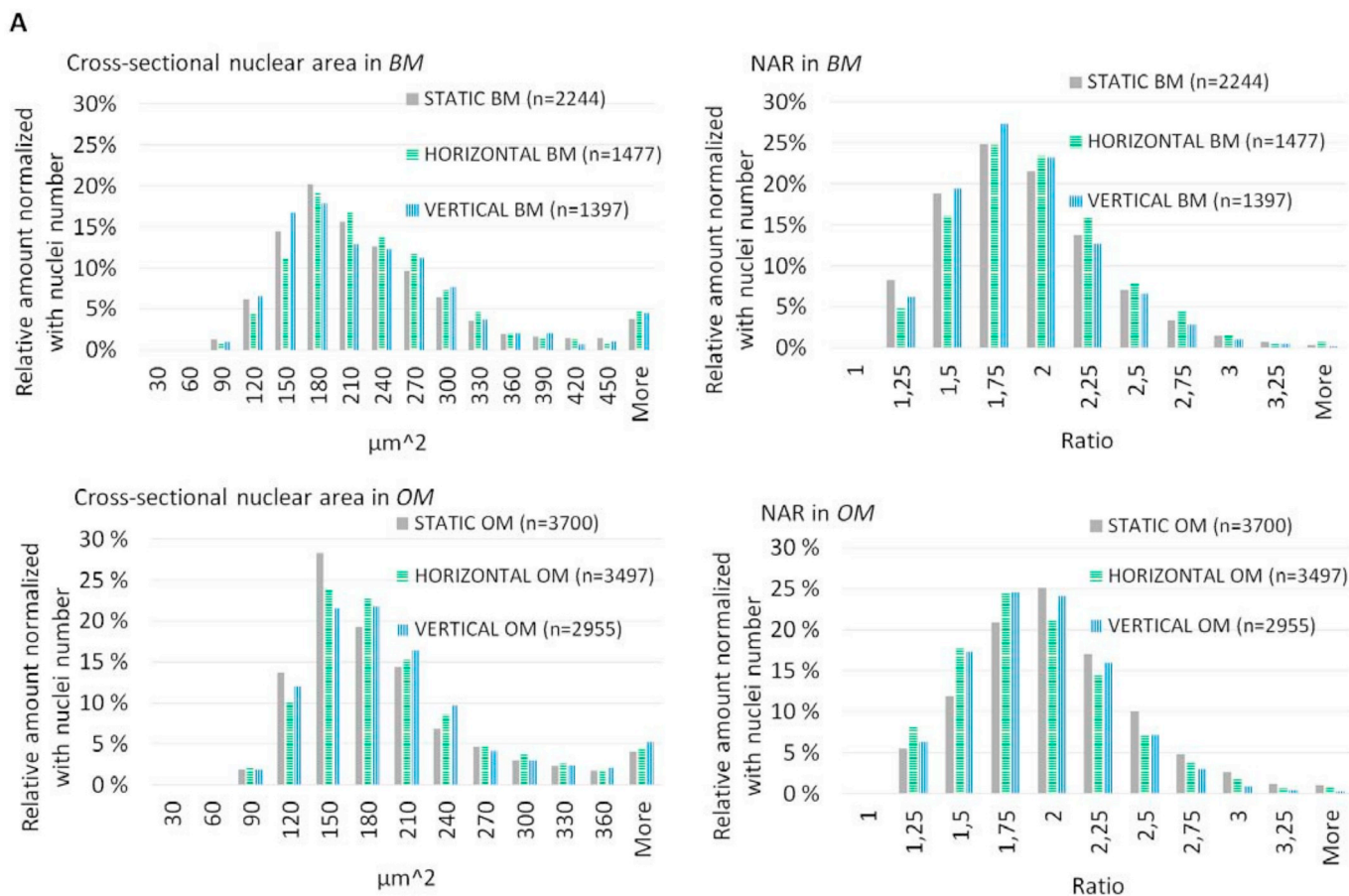

Fig. 5. Nuclear morphology of the hASCs in static culture, horizontal stimulation, and vertical stimulation conditions in *BM* and *OM* on the asTCP surface at day 11. (A): The nuclear morphology distributions, after normalizing to total nuclei counts. Data are presented as clustered columns of the nuclear area and the nuclear aspect ratio (*NAR*), together with nuclei count (n). (B): The nuclear area and *NAR* values after excluding the nuclei exceeding the upper outliers (+2 *SD* cross-sectional nuclear area). Data are presented as box plots together with nuclei count (n). Comparisons are made between the static culture and HMHF vibrated conditions (α, horizontal; β vertical) and between the horizontal and vertical stimulation conditions (γ). *, p < 0.05, **, p < 0.01, ***, p < 0.001.

(Nikukar et al., 2013; Uzer et al., 2015; Zhang et al., 2015), and the combinatory effects of vibration and biochemically-induced differentiation remain understudied (Demiray and Özcivici, 2015). Our aim was to study the horizontal and vertical HMHF vibration in hASCs because their mechanoresponsivity has been demonstrated to differ from that of hBMSCs (Choi et al., 2012; Bartlett et al., 2015). First, we analyzed the proliferation and osteogenic differentiation on standard and cell adhesion supporting surfaces. After observing the importance of cell adhesion on HF vibration responses, we evaluated the actin cytoskeleton and the nuclei on the cell adhesion supporting surfaces using image-based analysis methods. Our current findings provide new knowledge on the synergistic effects of mechanical and biochemical stimuli in directing the biophysical responses of hASCs in different culture conditions.

4.1. HMHF vibration as a mechanical stimulus

The high-throughput cell stimulators we developed enabled us to perform long-term experiments in standard cell culture conditions. This allowed us to apply the stimulation bouts automatically without affecting the culture environment, in contrast to prior studies that conducted stimulation outside the incubators (Sen et al., 2011; Kim et al., 2012; Uzer et al., 2015; Pongkitwitoon et al., 2016). The vibration protocol comprised several stimulation bouts daily, which has been demonstrated to be beneficial for cell responses (Sen et al., 2011; Uzer et al., 2015). In addition, we applied HMHF vibration, which increases the inertial force-related nuclear displacements, as proposed by mathematical models (Uzer et al., 2014; Wang et al., 2016). Furthermore, we applied the stimulus with high frequency, which efficiently decreases the fluid shear even at high magnitudes (Uzer et al., 2012, 2013). We consider that the mechanical stimulus of the HMHF vibration occurred mostly through the inertial forces of the nuclear displacements. However, some fluid shear-specific differentiation responses to the HF vibration have been reported (Uzer et al., 2013; Pongkitwitoon et al., 2016). Thus, fluid shear might have secondary effects. Changes in cell morphology (Wang et al., 2016) and cellular stiffness (Uzer et al., 2014) are capable of altering the nuclear displacements with HF vibration, as suggested by the mathematical models. Consequently, the cellular environment, through its guiding effects on the cell cytoskeleton and intracellular stiffness, is important both for the MSC differentiation process (Dalby et al., 2007a; Kilian et al., 2010; Walters and Gentleman, 2015) and for the mechanocoupling of the HF vibration stimulus (Uzer et al., 2015).

4.2. HMHF vibration effects on cell proliferation

Current knowledge on HF vibration induced proliferation is mostly based on studies conducted in *BM* condition, demonstrating highly varying stimulation effects on the cell number of the MSCs (Kim et al., 2012; Zhang et al., 2012, 2015; Pré et al., 2013; Uzer et al., 2013; Chen et al., 2015a; Pongkitwitoon et al., 2016). However, only a few studies have compared the effects of vibration in both *BM* and *OM* conditions (Tirkkonen et al., 2011; Demiray and Özcivici, 2015; Lu et al., 2018). In this present study, we analyzed the cell proliferation of hASCs in *BM* and *OM* conditions to provide complementary knowledge on the effects of HMHF vibration in these culture conditions combined with different cell culture surfaces because there is some evidence that HF vibration induced proliferation is even enhanced with improved cell adhesion (Uzer et al., 2013). Based on our findings, neither horizontal nor vertical HMHF vibration had an effect on cell proliferation on the sTCP surface. This is in line with our previous results with the vertical HMHF vibration of the hASCs (Tirkkonen et al., 2011). The improved adhesion generated by the asTCP surface allowed us to see the effects of the culture media in combination with the vibration response. In *BM* condition, both stimulation directions diminished proliferation compared with the static culture condition. This contrasts with the findings of

Pongkitwitoon and co-workers who reported that both stimulation directions induced proliferation, the horizontal stimulation being the more beneficial (Pongkitwitoon et al., 2016). In *OM* condition, we saw a difference between the horizontal and vertical stimulation directions, but there was a donor-dependent response when compared with the static culture. In general, the discrepancy between studies may be due to the variance between the culture and stimulation parameters used.

4.3. HMHF vibration effects on osteogenic differentiation

Previous studies have found that HF vibration is beneficial for the osteogenic differentiation of MSCs regardless of the stimulation parameter combinations used (Pré et al., 2011, 2013; Tirkkonen et al., 2011; Kim et al., 2012; Uzer et al., 2013; Pongkitwitoon et al., 2016; Maredziak et al., 2017; Lu et al., 2018). Osteogenic differentiation is characterized by the early expression of ALP, which declines with the expression of other osteogenic genes and mineralization processes (Golub and Boesze-Battaglia, 2007). Interestingly, the early activitation of ALP also occurs with the HF vibration (Tirkkonen et al., 2011; Kim et al., 2012; Lu et al., 2018). Pongkitwitoon and co-workers were the first to report that especially horizontal, but also vertical HF vibration enhanced the ALP activity of hBMSCs (Pongkitwitoon et al., 2016). In the present study, we discovered a similar effect with two donors on the sTCP surface at the 18 day time point, although the effect was statistically not significant. On the adhesion supporting surface, however, the vibration effect was already evident at the 14 day time point. The horizontal stimulation boosted ALP activity, but vertical stimulation had an inhibitory effect. To the best of our knowledge, this is the first study that shows that the HF vibration -mediated ALP activity of MSCs was altered by supporting the cell adhesion mechanism with a culture surface designed to improve cell attachment (Pardo et al., 2005). Moreover, cell adhesion and FAK mediated signaling are considered important for the osteogenic differentiation of MSCs (Salasznyk et al., 2007; Shih et al., 2011; Hyväri et al., 2018). FAK is a central protein in "outside-in" signaling providing a connection between the extracellular matrix (ECM) and the cell cytoskeleton (Legate et al., 2009). In addition, FAK mediated signaling has also been linked to the mechanocoupling of HF vibration (Nikukar et al., 2013; Uzer et al., 2015). Our results suggest that horizontal stimulation is capable of intensifying ALP activity and more focus should be given to this stimulation direction in combination with culture surface properties.

To further study the osteogenic differentiation, we analyzed the matrix mineralization of the HMHF vibrated hASCs. Our results show that the mineral accumulation increased with time. Mineralization appeared stronger on the asTCP surface, although no clear HMHF vibration induced benefits occurred. Previously, horizontal HF vibration has been shown to intensify the mineral accumulation of hBMSCs more than vertical stimulation (Pongkitwitoon et al., 2016). Interestingly, HF vibration-related mineralization has also correlated with the ALP activity responses of MSCs (Kim et al., 2012; Pongkitwitoon et al., 2016; Lu et al., 2018). However, we found a similar response with only one donor on the asTCP surface. Previous studies have reported that mineralization responses to HF vibration are dependent on the length of the culture (Pré et al., 2011, 2013; Chen et al., 2015a; Pongkitwitoon et al., 2016). In our study, we also found that the mineralization of hASCs responds differently to HMHF vibration at different time points. According to Chen and co-workers, this phenomenon could be due to the ongoing osteogenic differentiation, which alters the crucial mechanosensors (Chen et al., 2015a).

4.4. HMHF vibration effects on the actin cytoskeleton

We performed image-based analysis to quantitatively classify phalloidin-TRITC-stained actin cytoskeleton. We found that the culture medium played a role in the reorganization of the actin cytoskeleton because the *OM* condition contained more criss-crossed structures in

both static culture and horizontal stimulation conditions than the *BM* condition. These results are in line with our findings on ALP activity, and indicate the importance of the actin cytoskeleton on the osteogenic course. Osteogenesis has been characterized by the criss-crossed pattern of actin (Yourek et al., 2007) and increased cellular stiffness (Yourek et al., 2007; Darling et al., 2008). According to our findings, the horizontal stimulation increased the parallel alignment of the hASCs according to the stimulation direction in *OM* condition. Similar findings were also reported in a previous study after only 1 day of stimulation of hBMSCs with horizontal LMHF vibration (Pongkitwitoon et al., 2016). In contrast, we found vertical stimulation enhanced the amount of randomly organized actin at the cost of the criss-crossed actin. Additionally, vertical stimulation decreased the coherency of the parallel-aligned actin filaments. This might lead to lowered tension, and thus result in decreased ALP activity of the hASCs with this stimulation direction. Taken together, our results indicate that the organization of the actin cytoskeleton could be used as an indicator of osteogenesis.

4.5. HMHF vibration effects on the nuclei

The morphology of the DAPI-stained nuclei were studied to elucidate the HMHF vibration related "inside-inside" signaling mechanism, occurring through nuclear movements (Uzer et al., 2015). Nuclear deformations of MSCs have been studied using cell stretching (Heo et al., 2015, 2016), a dynamic culture method also used in osteogenic differentiation (Virjula et al., 2017). The results of our study show that nuclear size decreased notably in static *OM* condition when compared with *BM* condition. Additionally, we found more elongated nuclei in the osteogenically induced hASCs. Our results are supported by previous findings suggesting that the nuclei of mature osteoblasts are more elongated than with osteoblast precursors (Zouani et al., 2013). Furthermore, similar nuclear morphology changes to our findings have also been reported after 10 days of adipogenic differentiation of porcine MSCs (Stachecka et al., 2018). Interestingly, HMHF vibration reduced the biochemically induced changes in the nuclear size and elongation of hASCs in *OM* condition. Our results add knowledge to the increased nuclear height as a response to HF vibration reported by Demiray and Özcivici (2015). The nuclear morphology is dependent on the cellular tensile state (Dalby et al., 2007b; Chen et al., 2015b) and the actin cap (Khatau et al., 2009), but also on the intranuclear architecture, such as intranuclear actin (Sen et al., 2017), nuclear lamin, and chromatin condensation (Heo et al., 2016). During differentiation intranuclear structures change (Ihalainen et al., 2015; Heo et al., 2016; Sen et al., 2017) and nuclear stiffness increases (Pajerowski et al., 2007; Heo et al., 2016). These changes in nuclear mechanics could also affect the mechanocoupling of the HF vibration by affecting the nuclear movement in the cell. Indeed, they could explain our observation that the nuclear morphology changes in HMHF vibration during osteogenic differentiation.

5. Conclusion

In this study, we have developed high-throughput stimulators using 3D printing to provide new information on how HMHF vibration direction effects the proliferation, osteogenesis, and cellular organization of hASCs. Our central findings indicate that cell adhesion is a prerequisite for the HMHF vibration induced proliferation and early osteogenesis, possibly denoting the importance of adhesion-mediated mechanotransduction. On the adhesion supporting culture platform, horizontal stimulation was found to be beneficial, but vertical stimulation inhibitory for ALP activity. The HMHF vibration failed to induce maturation towards the bone cells. We found culture condition dependent effects on the intracellular structures with ICC staining. The horizontal stimulation aligned the actin cytoskeleton in *OM* condition according to the stimulation direction, whereas the vertical stimulation decreased the coherency of the actin filaments. The nuclei responded

especially to the biochemically induced osteogenic induction, whereas both stimulation directions modestly reduced this effect. Taken together, our results indicate that the horizontal stimulation should be recognized as a more desirable alternative to the vertical stimulation. The HF vibration responses could be tuned by supporting the cell adhesion mechanism, for example, by optimizing the culture surface. However, further studies on the intranuclear architecture and its role in the mechanocoupling would be beneficial.

Conflicts of interest

The authors declare no conflict of interests.

Appendix A. Supplementary data

Supplementary data to this article can be found online at https://doi.org/10.1016/j.jmbbm.2019.103419.

References

Bartlett, R.S., Gaston, J.D., Yen, T.Y., Ye, S., Kendziorski, C., Thibeault, S.L., 2015. Biomechanical screening of cell therapies for vocal fold scar. Tissue Eng. A 21, 2437–2447. https://doi.org/10.1089/ten.TEA.2015.0168.

Berens, P., 2009. CircStat: a MATLAB toolbox for circular Statistics. J. Stat. Softw Sep, 31. https://doi.org/10.18637/jss.v031.i10.

Chen, X., He, F., Zhong, D.Y., Luo, Z.P., 2015a. Acoustic-frequency vibratory stimulation regulates the balance between osteogenesis and adipogenesis of human bone marrow-derived mesenchymal stem cells. BioMed Res. Int. 540731. https://doi.org/10.1155/2015/540731.

Chen, B., Co, C., Ho, C.C., 2015b. Cell shape dependent regulation of nuclear morphology. Biomaterials 67, 129–136. https://doi.org/10.1016/j.biomaterials.2015.07.017.

Choi, Y.S., Vincent, L.G., Lee, A.R., Dobke, M.K., Engler, A.J., 2012. Mechanical derivation of functional myotubes from adipose-derived stem cells. Biomaterials 33, 2482–2491. https://doi.org/10.1016/j.biomaterials.2011.12.004.

Cui, H., Nowicki, M., Fisher, J.P., Zhang, L.G., 2017. 3D bioprinting for organ regeneration. Adv. Healthc. Mater. 6. https://doi.org/10.1002/adhm.201601118.

Dalby, M.J., Gadegaard, N., Tare, R., Andar, A., Riehle, M.O., Herzyk, P., Wilkinson, C.D.W., Oreffo, R.O.C., 2007a. The control of human mesenchymal cell differentiation using nanoscale symmetry and disorder. Nat. Mater. 6, 997–1003. https://doi.org/10.1038/nmat2013.

Dalby, M.J., Biggs, M.J.P., Gadegaard, N., Kalna, G., Wilkinson, C.D.W., Curtis, A.S.G., 2007b. Nanotopographical stimulation of mechanotransduction and changes in interphase centromere positioning. J. Cell. Biochem. 100, 326–338. https://doi.org/10.1002/jcb.21058.

Darling, E.M., Topel, M., Zauscher, S., Vail, T.P., Guilak, F., 2008. Viscoelastic properties of human mesenchymally-derived stem cells and primary osteoblasts, chondrocytes, and adipocytes. J. Biomech. 41, 454–464. https://doi.org/10.1016/j.jbiomech.2007.06.019.

Demiray, L., Özcivici, E., 2015. Bone marrow stem cells adapt to low-magnitude vibrations by altering their cytoskeleton during quiescence and osteogenesis. Turk. J. Biol. 39, 88–97. https://doi.org/10.3906/biy-1404-35.

Dodziuk, H., 2016. Applications of 3D printing in healthcare. Pol. J. Cardiothorac. Surg. 13, 283–293. https://doi.org/10.5114/kitp.2016.62625.

Dominici, M., Le Blanc, K., Mueller, I., Slaper-Cortenbach, I., Marini, F.C., Krause, D.S., Deans, R.J., Keating, A., Prockop, D.J., Horwitz, E.M., 2006. Minimal criteria for

defining multipotent mesenchymal stromal cells. The International Society for Cellular Therapy position statement. Cytotherapy 8, 315–317. https://doi.org/10.1080/14653240600855905.

Edwards, J.H., Reilly, G.C., 2015. Vibration stimuli and the differentiation of musculoskeletal progenitor cells: review of results in vitro and in vivo. World J. Stem Cells 7, 568–582. https://doi.org/10.4252/wjsc.v7.i3.568.

Golub, E., Boesze-Battaglia, K., 2007. The role of alkaline phosphatase in mineralization. Curr. Opin. Orthop. 18, 444–448. https://doi.org/10.1097/BCO.0b013e3282630851.

Halonen, H.T., Hyttinen, J.A.K., Ihalainen, T.O., 2020. Miniaturized stimulator for imaging of live cell responses to high frequency mechanical vibration. In: In: Badnjevic, A., Skribic, R., Gurbeta, P.L. (Eds.), CMBEBIH 2019. IFMBE Proceedings, vol. 73. Springer, Cham, pp. 21–27. https://doi.org/10.1007/978-3-030-17971-7_4.

Heo, S.J., Thorpe, S.D., Driscoll, T.P., Duncan, R.L., Lee, D.A., Mauck, R.L., 2015. Biophysical regulation of chromatin architecture instills a mechanical memory in mesenchymal stem cells. Sci. Rep. 5, 16895. https://doi.org/10.1038/srep16895.

Heo, S.J., Driscoll, T.P., Thorpe, S.D., Nerurkar, N.L., Baker, B.M., Yang, M.T., Chen, C.S., Lee, D.A., Mauck, R.L., 2016. Differentiation alters stem cell nuclear architecture, mechanics, and mechanosensitivity. Elife 5, e18207. https://doi.org/10.7554/eLife.18207.

Hyväri, L., Ojansivu, M., Juntunen, M., Kartasalo, K., Miettinen, S., Vanhatupa, S., 2018. Focal adhesion kinase and ROCK signaling are switch-like regulators of human adipose stem cell differentiation towards osteogenic and adipogenic lineages. Stem Cell. Int 2190657. https://doi.org/10.1155/2018/2190657.

Ihalainen, T.O., Aires, L., Herzog, F.A., Schwartlander, R., Moeller, J., Vogel, V., 2015. Differential basal-to-apical accessibility of lamin A/C epitopes in the nuclear lamina regulated by changes in cytoskeletal tension. Nat. Mater. 14, 1252–1261. https://doi.org/10.1038/nmat4389.

Kartasalo, K., Pölönen, R.P., Ojala, M., Rasku, J., Lekkala, J., Aalto-Setälä, K., Kallio, P., 2015. CytoSpectre: a tool for spectral analysis of oriented structures on cellular and subcellular levels. BMC Bioinf. 16 344. https://doi.org/10.1186/s12859-015-0782-y.

Khatau, S.B., Hale, C.M., Stewart-Hutchinson, P.J., Patel, M.S., Stewart, C.L., Searson, P.C., Hodzic, D., Wirtz, D., 2009. A perinuclear actin cap regulates nuclear shape. Proc. Natl. Acad. Sci. U.S.A. 106 19017–22. https://doi.org/10.1073/pnas.0908686106.

Kilian, K.A., Bugarija, B., Lahn, B.T., Mrksich, M., 2010. Geometric cues for directing the differentiation of mesenchymal stem cells. Proc. Natl. Acad. Sci. U.S.A. 107, 4872–4877. https://doi.org/10.1073/pnas.0903269107.

Kim, I.S., Song, Y.M., Lee, B., Hwang, S.J., 2012. Human mesenchymal stromal cells are mechanosensitive to vibration stimuli. J. Dent. Res. 91, 1135–1140. https://doi.org/10.1177/0022034512465291.

Kim, H.J., Kim, J.H., Song, Y.J., Seo, Y.K., Park, J.K., Kim, C.W., 2015. Overexpressed calponin3 by subsonic vibration induces neural differentiation of hUC-MSCs by regulating the ionotropic glutamate receptor. Appl. Biochem. Biotechnol. 177, 48–62. https://doi.org/10.1007/s12010-015-1726-8.

Lau, E., Lee, W.D., Li, J., Xiao, A., Davies, J.E., Wu, Q., Wang, L., You, L., 2011. Effect of low-magnitude, high-frequency vibration on osteogenic differentiation of rat mesenchymal stromal cells. J. Orthop. Res. 29, 1075–1080. https://doi.org/10.1002/jor.21334.

Lavrov, A.V., Smirnikhina, S.A., 2010. Nuclear heterogeneity and proliferation activity of human adipose derived MSC-like cells. Cell Tissue Biol. 4, 452. https://doi.org/10.1134/S1990519X1005007X.

Legate, K., Wickström, S.A., Fässler, R., 2009. Genetic and cell biological analysis of integrin outside-in signaling. Genes Dev. 23, 397–418. https://doi.org/10.1101/gad.1758709.

Lu, Y., Zhao, Q., Liu, Y., Zhang, L., Li, D., Zhu, Z., Gan, X., Yu, H., 2018. Vibration loading promotes osteogenic differentiation of bone marrow-derived mesenchymal stem cells via p38 MAPK signaling pathway. J. Biomech. 71, 67–75. https://doi.org/10.1016/j.jbiomech.2018.01.039.

Marediak, M., Lewandowski, D., Tomaszewski, K.A., Kubiak, K., Marycz, K., 2017. The effect of low-magnitude low-frequency vibration (LMLF) on osteogenic differentiation potential of human adipose derived mesenchymal stem cells. Cell. Mol. Bioeng. 10, 549–562. https://doi.org/10.1007/s12195-017-0501-z.

Marycz, K., Lewandowski, D., Tomaszewski, K.A., Henry, B.M., Golec, E.B., Marediak, M., 2016. Low-frequency, low-magnitude vibrations (LFLM) enhances chondrogenic differentiation potential of human adipose derived mesenchymal stromal cells (hASCs). PeerJ 4 e1637. https://doi.org/10.7717/peerj.1637.

McClarren, B., Olabisi, R., 2018. Strain and vibration in mesenchymal stem cells. Int. J. Biom 8686794. https://doi.org/10.1155/2018/8686794.

Nikander, R., Kannus, P., Dastidar, P., Hannula, M., Harrison, L., Cervinka, T., Narra, N.G., Aktour, R., Arola, T., Eskola, H., Soimakallio, S., Heinonen, A., Hyttinen, J., Sievänen, H., 2009. Targeted exercises against hip fragility. Osteoporos. Int. 20, 1321–1328. https://doi.org/10.1007/s00198-008-0785-x.

Nikukar, H., Reid, S., Tsimbouri, P.M., Riehle, M.O., Curtis, A.S.G., Dalby, M.J., 2013. Osteogenesis of mesenchymal stem cells by nanoscale mechanotransduction. ACS Nano 7, 2758–2767. https://doi.org/10.1021/nn400202j.

Pajerowski, J.D., Dahl, K.N., Zhong, F.L., Sammak, P.J., Discher, D.E., 2007. Physical plasticity of the nucleus in stem cell differentiation. Proc. Natl. Acad. Sci. U.S.A. 104, 15619–15624. https://doi.org/10.1073/pnas.0702576104.

Paluch, E.K., Nelson, C.M., Biais, N., Fabry, B., Moeller, J., Pruitt, B.L., Wollnik, C., Kudryasheva, G., Rehfeldt, F., Federle, W., 2015. Mechanotransduction: use of the force(s). BMC Biol. 13 47. https://doi.org/10.1186/s12915-015-0150-4.

Pardo, A.M.P., Bryan, M., Krasnow, H., Hardin, M., Riddle, M., LaChance, O., Gagnon, P., Upton, T., Hoover, D.S., 2005. Corning® CellBIND® Surface: An improved surface for enhanced cell attachment. Corning Incorporated. https://www.zenonbio.hu/docs/cellbind_improved_surface.pdf, Accessed date: 7 September 2019.

Pemberton, G.D., Childs, P., Reid, S., Nikukar, H., Tsimbouri, P.M., Gadegaard, N., Curtis, A.S.G., Dalby, M.J., 2015. Nanoscale stimulation of osteoblastogenesis from mesenchymal stem cells: nanotopography and nanokicking. Nanomedicine 10, 547–560. https://doi.org/10.2217/nnm.14.134.

Pongkitwitoon, S., Uzer, G., Rubin, J., Judex, S., 2016. Cytoskeletal configuration modulates mechanically induced changes in mesenchymal stem cell osteogenesis, morphology, and stiffness. Sci. Rep. 6 34791. https://doi.org/10.1038/srep34791.

Pré, D., Ceccarelli, G., Gastaldi, G., Asti, A., Saino, E., Visai, L., Benazzo, F., Cusella De Angelis, M.G., Magenes, G., 2011. The differentiation of human adipose-derived stem cells (hASCs) into osteoblasts is promoted by low amplitude, high frequency vibration treatment. Bone 49, 295–303. https://doi.org/10.1016/j.bone.2011.04.013.

Pré, D., Ceccarelli, G., Visai, L., Benedetti, L., Imbriani, M., Cusella De Angelis, M.G., Magenes, G., 2013. Clinical study: high-frequency vibration treatment of human bone marrow stromal cells increases differentiation toward bone tissue. Bone Marrow Res. 803450. https://doi.org/10.1155/2013/803450.

Raveling, A.R., Theodossiou, S.K., Schiele, N.R., 2018. A 3D printed mechanical bioreactor for investigating mechanobiology and soft tissue mechanics. Methods 5, 924–932. https://doi.org/10.1016/j.mex.2018.08.001.

Salasznyk, R.M., Klees, R.F., Williams, W.A., Boskey, A., Plopper, G.E., 2007. Focal adhesion kinase signaling pathways regulate the osteogenic differentiation of human mesenchymal stem cells. Exp. Cell Res. 313, 22–37. https://doi.org/10.1016/j.yexcr.2006.09.013.

Sen, B., Xie, Z., Case, N., Styner, M., Rubin, C.T., Rubin, J., 2011. Mechanical signal influence on mesenchymal stem cell fate is enhanced by incorporation of refractory periods into the loading regimen. J. Biomech. 44, 593–599. https://doi.org/10.1016/j.jbiomech.2010.11.022.

Sen, B., Uzer, G., Samsonraj, R.M., Xie, Z., McGrath, C., Styner, M., Dudakovic, A., van Wijnen, A.J., Rubin, J., 2017. Intranuclear actin structure modulates mesenchymal stem cell differentiation. Stem Cells 35, 1624–1635. https://doi.org/10.1002/stem.2617.

Shih, Y.R., Tseng, K.F., Lai, H.Y., Lin, C.H., Lee, O.K., 2011. Matrix stiffness regulation of integrin-mediated mechanotransduction during osteogenic differentiation of human mesenchymal stem cells. J. Bone Miner. Res. 26, 730–738. https://doi.org/10.1002/jbmr.278.

Stachecka, J., Walczak, A., Kociucka, B., Ruszczycki, B., Wilczynski, G., Szczerbal, I., 2018. Nuclear organization during in vitro differentiation of porcine mesenchymal stem cells (MSCs) into adipocytes. Histochem. Cell Biol. 149, 113–126. https://doi.org/10.1007/s00418-017-1618-9.

Tirkkonen, L., Halonen, H., Hyttinen, J., Kuokkanen, H., Sievänen, H., Koivisto, A.M., Mannerström, B., Sándor, G.K.B., Suuronen, R., Miettinen, S., Haimi, S., 2011. The effects of vibration loading on adipose stem cell number, viability and differentiation towards bone-forming cells. J. R. Soc. Interface 8, 1736–1747. https://doi.org/10.1098/rsif.2011.0211.

Tirkkonen, L., Haimi, S., Huttunen, S., Wolff, J., Pirhonen, E., Sándor, G.K.B., Miettinen, S., 2013. Osteogenic medium is superior to growth factors in differentiation of human adipose stem cells towards bone-forming cells in 3D culture. Eur. Cells Mater. 25, 144–158. https://doi.org/10.22203/eCM.v025a10.

Titushkin, I., Cho, M., 2007. Modulation of cellular mechanics during osteogenic differentiation of human mesenchymal stem cells. Biophys. J. 93, 3693–3702. https://doi.org/10.1529/biophysj.107.107797.

Uzer, G., Manske, S.L., Chan, M.E., Chiang, F.P., Rubin, C.T., Frame, M.D., Judex, S., 2012. Separating fluid shear stress from acceleration during vibration in vitro: identification of mechanical signals modulating the cellular response. Cell. Mol. Bioeng. 5, 266–276. https://doi.org/10.1007/s12195-012-0231-1.

Uzer, G., Pongkitwitoon, S., Ete Chan, M., Judex, S., 2013. Vibration induced osteogenic commitment of mesenchymal stem cells is enhanced by cytoskeletal remodeling but not fluid shear. J. Biomech. 46, 2296–2302. https://doi.org/10.1016/j.jbiomech.2013.06.008.

Uzer, G., Pongkitwitoon, S., Ian, C., Thompson, W.R., Rubin, J., Chan, M.E., Judex, S., 2014. Gap junctional communication in osteocytes is amplified by low intensity vibration in vitro. PLoS One 9, e90840. https://doi.org/10.1371/journal.pone.0090840.

Uzer, G., Thompson, W.R., Sen, B., Xie, Z., Yen, S.S., Miller, S., Bas, G., Styner, M., Rubin, C.T., Judex, S., Burridge, K., Rubin, J., 2015. Cell mechanosensitivity to extremely low magnitude signals is enabled by a LINCed nucleus. Stem Cells 33, 2063–2076. https://doi.org/10.1002/stem.2004.

Varma, M.J., Breuls, R.G.M., Schouten, T.E., Jurgens, W.J.F.M., Bontkes, H.J., Schuurhuis, G.J., Van Ham, S.M., Van Milligen, F.J., 2007. Phenotypical and functional characterization of freshly isolated adipose tissue-derived stem cells. Stem Cells Dev. 16, 91–104. https://doi.org/10.1089/scd.2006.0026.

Verschueren, S.M.P., Roelants, M., Delecluse, C., Swinnen, S., Vanderschueren, D., Boonen, S., 2004. Effect of 6-month whole body vibration training on hip density, muscle strength, and postural control in postmenopausal women: a randomized controlled pilot study. J. Bone Miner. Res. 19, 352–359. https://doi.org/10.1359/JBMR.0301245.

Virjula, S., Zhao, F., Leivo, J., Vanhatupa, S., Kreutzer, J., Vaughan, T.J., Honkala, A.M., Viehrig, M., Mullen, C.A., Kallio, P., McNamara, L.M., Miettinen, S., 2017. The effect of equiaxial stretching on the osteogenic differentiation and mechanical properties of human adipose stem cells. J. Mech. Behav. Biomed. Mater. 72, 38–48. https://doi.org/10.1016/j.jmbbm.2017.04.016.

Walters, N.J., Gentleman, E., 2015. Evolving insights in cell-matrix interactions: elucidating how non-soluble properties of the extracellular niche direct stem cell fate. Acta Biomater. 11, 3–16. https://dx.doi.org/10.1016/j.actbio.2014.09.038.

Wang, L., Hsu, H.Y., Li, X., Xian, C.J., 2016. Effects of frequency and acceleration amplitude on osteoblast mechanical vibration responses: a finite element study. BioMed

Res. Int 2735091. https://dx.doi.org/10.1155/2016/2735091.

Yourek, G., Hussain, M.A., Mao, J.J., 2007. Cytoskeletal changes of mesenchymal stem cells during differentiation. Am. Soc. Artif. Intern. Organs J. 53, 219–228. https://doi.org/10.1097/MAT.0b013e31802deb2d.

Zhang, C., Li, J., Zhang, L., Zhou, Y., Hou, W., Quan, H., Li, X., Chen, Y., Yu, H., 2012. Effects of mechanical vibration on proliferation and osteogenic differentiation of human periodontal ligament stem cells. Arch. Oral Biol. 57, 1395–1407. https://doi.org/10.1016/j.archoralbio.2012.04.010.

Zhang, C., Lu, Y., Zhang, L., Liu, Y., Zhou, Y., Chen, Y., Yu, H., 2015. Influence of different intensities of vibration on proliferation and differentiation of human periodontal ligament stem cells. Arch. Med. Sci. 11, 638–646. https://doi.org/10.5114/aoms.2015.52370.

Zhao, Q., Lu, Y., Gan, X., Yu, H., 2017. Low magnitude high frequency vibration promotes adipogenic differentiation of bone marrow stem cells via P38 MAPK signal. PLoS One 12, e0172954. https://doi.org/10.1371/journal.pone.0172954.

Zouani, O.F., Rami, L., Lei, Y., Durrieu, M.C., 2013. Insights into the osteoblast precursor differentiation towards mature osteoblasts induced by continuous BMP-2 signaling. Open Biol. 2, 872–881. https://doi.org/10.1242/bio.20134986.